Frequency Selective Surfaces offer new possibilities as reflectance filters in the NIR/visible spectrum

Gary F. Walsh[a], Richard M. Osgood III[a], David Ziegler[a], Madhumita Roy[b], Joel Carlson[a], Lauren Belton[a], and Brian R. Kimball[*a]

[a]Nanomaterials Science Team, U. S. Army Natick Soldier Research Development and Engineering Center, Natick, MA 01760
[b]Sensors and Electron Devices Directorate, U.S. Army Research Laboratory
2800 Powder Mill Road, Adelphi, Maryland 20783

ABSTRACT

Frequency Selective Surfaces (FSS) are comprised of periodic, geometric, metallic patterns that act like an array of horizontal antennas. They were originally designed as band-pass/band-block filters. Nanofabrication techniques allow for the realization of FSS structures that operate in the near infrared (NIR) and visible portions of the electromagnetic spectrum. Thus it is possible to create arrays of light antenna filters possessing optical properties that are unlike those of dye, dielectric, or holographic filters that are in common use today. Recent studies of arrays of gold, dipole nanoantennas by our group and others offer an opportunity to compare modeled FSS response with experimental results elucidating the unique, off-normal reflectance stability of frequency selective surfaces operating in the NIR/visible portion of the spectrum.

Key Words: Frequency selective surface, periodic metallic nanostructures, band pass/band block filters, NIR/visible spectrum, optical properties, coupled dipoles.

1. INTRODUCTION

Frequency Selective Surfaces (FSSs) are composed of periodic arrays of metallic structures that can function as electromagnetic radiation filters. There are two general types of FSSs: inductive FSSs, comprised of periodic holes in a conductive sheet, and capacitive FSSs, comprised of periodic antennae in a dielectric medium[1,2]. Inductive FSSs act as band pass filters exhibiting peaks in transmission at their resonance frequency, while capacitive FSSs act as band stop filters with peaks in reflection[1,2]. These structures were first theorized in the early 1900s and have been used extensively since the 1960s[1]. Much work has been done over the past forty years to optimize their design for use as filters and dichroic mirrors in the RF and microwave portions of the spectrum. The fast role off and favorable off-normal performance that has been demonstrated with these devices suggests that they could be useful for applications in the optical regime. However, since their dimensions must be on the order of a fraction of a wavelength, until recently it has not been possible to construct FSSs that respond in the visible and near infrared (NIR). Optical inductive FSSs where first reported in 1998 by Ebbesen et. al. They observed that at certain wavelengths the absolute transmission efficiency through an array of periodically spaced subwavelength holes in a metallic sheet exceeded unity[6]. Over the past decade this phenomenon, known as extraordinary optical transmission, has been vigorously studied. As fabrication technology has continued to advance, it has become possible to make a variety of subwavelength structures with better control over size and spacing. This has enabled the production of optical capacitive FSSs[4].

Frequency Selective Surfaces provide the ability for the tailoring of spectral, polarization, and off-normal filtering responses in a way unparalleled by any technology available for use in the optical regime today. Many exotic geometries of both categories of FSSs have been combined with various dielectric covers and substrates to fine tune filters and dichroics with sharp role off, low or high polarization sensitivity, and good off-normal spectral uniformity.

Nanophotonic Materials V, edited by Zeno Gaburro, Stefano Cabrini, Dmitri Talapin
Proc. of SPIE Vol. 7030, 70300E, (2008) · 0277-786X/08/$18 · doi: 10.1117/12.795295

Before attempting to reproduce nano-scale versions of these complicated composite devices it is necessary to verify that the operation and theory of the most basic FSSs will scale appropriately. The simplest capacitive FSS is an infinite planar array of coupled dipole antennas with rectangular periodicity as shown in Figure 1. The intent of this study is to determine, for this basic geometry, the extent to which the circuit analogy used to design FSSs for RF and microwave applications holds in the visible and NIR. This design model will be further compared with the elegant theory of the coupling or hybridization of surface plasmons.

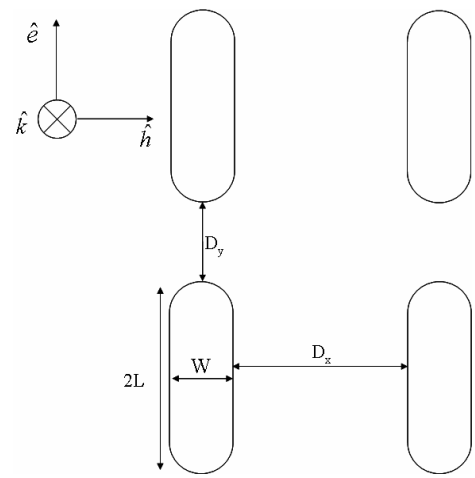

Figure 1: Four elements of an infinite planar array of dipole antennas with rectangular periodicity

2. THEORY

With the fabrication advancements that have made optical FSSs possible, it has become clear that the unique properties of arrays of metallic nanostructures can be used for a variety of applications beyond filtering. They have been used for high-resolution scanning near-field optical microscopy[3], detection of the surface enhanced raman scattering cross section of single molecules[4], making extremely small laser apertures[5], waveguiding systems[7] optical microscopy and lithography with resolution greater than the diffraction limit[23], and cancer treatments[8]. All of these applications are enabled by the large local field enhancement produced by the coupling of surface plasmons between adjacent nanoparticles[3-10].

Surface plasmons (SPs) are longitudinal waves of oscillating charges that propagate along a dielectric/conductor interface[9,11]. They are solutions to Maxwell's equations that are excited by transverse magnetic (TM) polarized light, and propagate parallel to the plain of incidence[11]. Equations 1 and 2 are the dispersion relations of SPs and photons, respectively[11], where k is the component of the wave vector in the direction of the plasmon, λ_0 is the free-space wavelength, ε_d and ε_m are the relative permittivities of the dielectric and metal respectively, and θ is the angle of incidence from the normal. These curves are illustrated in Figure 2.

$$k_{sp}(\lambda_0) = \frac{2\pi}{\lambda_0}\sqrt{\frac{\varepsilon_d \varepsilon_m}{\varepsilon_d + \varepsilon_m}} \tag{1}$$

$$k_p(\lambda_0) = \frac{2\pi}{\lambda_0}\sqrt{\varepsilon_d}\,\sin\theta \tag{2}$$

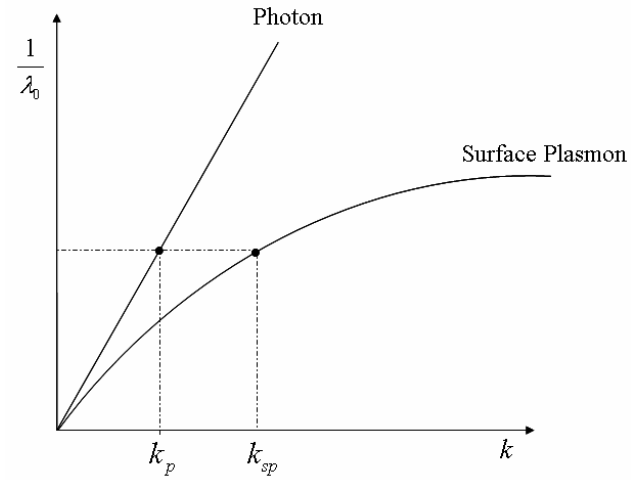

Figure 2: Dispersion relation of surface plasmons and photons

From Figure 2 it can be seen that a surface plasmon has a larger wave number (and therefore higher momentum, $p = k\hbar$) than a photon of the same frequency. In order for a photon to excite a SP it is necessary to compensate for this difference in momentum[9]. A standard method for doing this is to change the angle of incidence to increase the amount of momentum in the direction of SP propagation[11]. Another method is to form the metal surface into a periodic series of ridges and groves such as in a Bragg diffraction grating[9,13]. The periodicity makes up the difference in the wave vectors between the incident photons and the surface plasmons, thus satisfying the law of conservation of momentum. The Bragg condition is given in Equation 3 where $\Lambda_{x,y}$ are the periodicity of the grating in the x and y directions, and a and b are integers[6].

$$k_{SP} = k_P \pm a\frac{2\pi}{\Lambda_x} \pm b\frac{2\pi}{\Lambda_y} \tag{3}$$

The periodicity of the array functions as a two-dimensional Bragg coupler resulting in SPs propagating along the surface of the antennas. The discontinuity of the metal imposes the boundary condition that the current must be zero at all edges of each element analogous to that of a radio antenna[24]. Therefore a net oscillation of charge is possible only when the antenna is an integer multiple of the plasmon's half wavelength. These are the resonant modes of the antenna and the resonant frequency or wavelength from here on will refer to the lowest order mode corresponding to a length of half the plasmon's wavelength. At resonance, the boundary condition causes the charge density to be greatest at the ends of the antennas creating huge localized near-field enhancement many times larger then the incident optical field[3]. This enhancement will be greatest for plasmons propagating along the long axis of the antenna due to the small tip. This is also the reason the edges in our design are rounded rather than square. As the polarity of the antennas oscillates, they reradiate the energy they have captured from the incident field. The close proximity of the antennas causes their radiated fields to interact. Unlike photons, plasmons are affected by electromagnetic fields, because their energy is stored in the oscillation of electrons. When the radiated field from one antenna reaches its neighbor, it effects the oscillation of its electrons, which results in a shift in the resonance frequency of the plasmons[18]. This phenomenon is termed the coupling or hybridization[10] of plasmons between adjacent elements and is the fundamental mechanism underlying the extraordinary reflection properties of capacitive FSSs.

To design FSSs for RF and microwave applications, engineers have developed an analogous circuit theory. A dipole antenna is modeled by two inductors on either side of an AC current source. The coupling between antennas in the direction of the current is represented as a capacitance -- hence the name capacitive FSS. The coupling along the axis orthogonal to the propagation direction of the plasmon adds an additional parasitic capacitance. This model is shown in Figure 3. Conversely, inductive FSSs are capacitive elements coupled together by inductances. Analyzing Figure 3 using the periodic moment method (PMM)[1], the reflection coefficient Γ = (E-reflected/E-incident) for an infinite planar array of dipole antennas illuminated by a TM polarized plane wave is:

$$\Gamma = \frac{-R_A}{(R_A + jX_A) + Z_L}. \tag{4}$$

Where R_A and X_A are the real and imaginary parts of the self-impedance of the array, and Z_L is the load impedance of a single coupled antenna (series LC impedance). It can be seen from Equation 4 that resonance occurs only when $Z_L = -jX_A$, meaning that the inductance and capacitance of each set of coupled antennae must perfectly tune out that of an arbitrarily chosen reference element coupled to the entire array. It also means that in order to have unity reflection, the antennas must posses no resistance. This presents a problem at optical frequencies where the conductivity of different metals varies greatly[19].

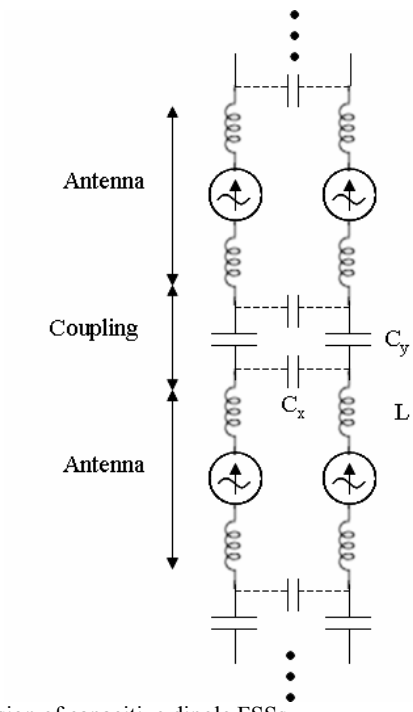

Figure 3: Analogous circuit model for design of capacitive dipole FSSs.

The trends relating resonance frequency to the size and spacing of the antennas can be expressed by the well-known equation for the resonance frequency of an LC circuit,

$$\omega = \frac{1}{\sqrt{LC}}, \tag{5}$$

where ω is the angular resonance frequency, L is the inductance, and C is the capacitance. A decrease in L and C will cause the resonance frequency to increase (blue shift). The inductance can be decreased directly by shortening the antennas or indirectly by shrinking the gap in the direction orthogonal to the plasmon, which will increase the parasitic capacitance. The capacitance can be reduced by increasing the gap along the parallel axis. It will be shown later that this is not universally true and that the electromagnetic coupled plasmon model is necessary to fully explain this relationship.

It is interesting to compare the reflectance properties of FSSs with the more traditional dielectric stack reflectance filter. The central wavelength of dielectric stack filters is determined by a resonance in vertical cavities. Such resonances are determined by the phase retardation induced each time the light travels through a layer. Changing the thickness of a layer alters the phase delay, which shifts the resonance. The distance traveled by the light in each layer changes with angle of incidence, therefore the effective thickness of the layers change, and so does the resonant wavelength. On the other

hand, FSS filters consist of horizontal cavities, so the length of the antennas determines their central wavelength. Changing the angle of incidence has no effect on their effective length. Therefore, the resonance frequency does not depend on angle of incidence. However, as can be seen from Equations 2 and 3, changing the angle of incidence does affect the coupling. In our simple dipole array this affects the width of the resonance peak.

Both R_A and Z_L in Equation 4 vary with launch angle. However, if D_x and D_y (in Figure 1) are small (<0.35λ), the change in X_A is also small and can be ignored[1]. Using this approximation, only the variation in R_A must be considered. R_A can be expressed for variations in either the E-k plane or the H-k plane depicted in Figure 4, where $\hat{k}$, $\hat{e}$, and $\hat{h}$ are the directions of $\vec{k}$, $\vec{E}$, and $\vec{H}$ at normal incidence for TM polarization.

For variations of launch angle θ in the E-k plane,

$$R_A = \frac{Z}{2D_x D_y} L^2 \cos\theta \,. \tag{6}$$

For variations of launch angle ϕ in the H-k plane,

$$R_A = \frac{Z}{2D_x D_y} \frac{L^2}{\cos\phi}, \tag{7}$$

where Z is the self impedance of a single element and L is half the antenna's length. An examination of Equation 4 shows that the full width half max (FWHM) of the resonance peak will get narrower as θ increases and wider as ϕ increases[1].

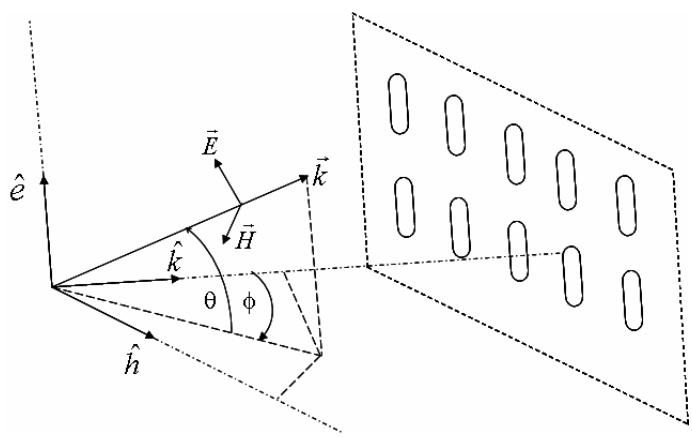

Figure 4: Coordinate system for illuminating dipole array

3. MODELING

We used rigorous coupled wave analysis (RCWA) simulations to verify visible and NIR far-field reflectivity findings reported by Smythe et. al.[4] for an array of gold nanoantennas illuminated by a TM polarized plane wave at normal incidence. We then used this model to verify the validity of the PMM off-normal formulas and to predict the surface polarization sensitivity. A model of an array of gold dipole antennas sitting on 22 nm of indium tin oxide (ITO) on a fused silica substrate was made using the complex refractive index values found in Palick's *Handbook of Optical Constant*[14]. Rigorous coupled wave analysis[15] simulations were performed using Li's inverse factoring algorithm for

periodic three-dimensional structures[16]. We examined the dependence of the far-field reflectance spectra on the length of the antennas (2L), the size of the gap along the long axis (D_y) and gap along the short axis (D_x). The simulations where performed by summing 13 harmonics along the long and short axes of the antennas and 13 Eigen modes. Resolution along the long and short axes was 0.005 μm ~ λ/150. The resolution in the direction of propagation was 0.01 μm ~ λ/75. It was found that the model produced results within 5% of those reported by Smythe for normal incidence. A similar model of thin gold and silver films in which surface plasmons were excited by scanning the angle of incidents agreed with reflectivity spectra reported by Sambles et. al.[11]. We concluded from these findings that the model was a practical tool for studying the off-normal properties of capacitive dipole FSSs in the visible and NIR.

Figure 5a shows the dependence of the absolute reflection efficiency[6] (the fraction of light reflected divided by the fraction of the surface covered by the antennas) on D_y. The antennas are 140 nm long, 60 nm wide, 50 nm thick, and the spacing along their short axis is 120 nm. As the spacing increases the peak blue shifts from 775 nm at D_y = 20 nm to 750 nm at D_y = 50 to 725 nm at D_y = 100 nm. Applying the circuit analogy, increasing this gap decreases the capacitive coupling, which increases the resonance frequency according to Equation 5. However, for gaps larger then 100 nm, the resonance frequency red shifts to 750 nm at D_y = 400 nm. Explaining this effect requires the use of coupled plasmon theory. The radiated field from the 'top' of one antenna will most strongly interact with that of the 'bottom' of its neighbor. When the antennas are separated by a distance that is less than about half the wavelength, these two fields will have the opposite sign and will add destructively which decreases their resonance frequency. As the antennas are moved farther apart this effect is less significant. However when the two are far enough apart (~λ/2), the radiated field undergoes a 180° phase shift before reaching its neighbor causing the fields to add constructively[4,17,18].

Figure 5b shows the dependence of the absolute reflection efficiency spectrum on D_x. The antennas are 80 nm long, 40 nm wide, 50 nm thick, and spaced 40 nm apart along their long axis. As the distance between the antennas is decreased there is a blue shift in the resonance frequency[4,18]. In terms of the circuit theory the reduced distance between the inductive elements (the antennas) increases the parasitic capacitance (C_x) which decreases L. This effect becomes greater as frequency is increased so it can be assumed to play a major role at optical frequencies. The decrease in inductance will increase the resonance frequency. In terms of the coupled plasmon model, the resonant fields of two parallel antennas resonating at the same frequency will add constructively leading to a higher resonance frequency.

Figure 5c shows the dependence of the absolute reflection efficiency spectrum on 2L. The antennas are 40 nm wide, and separated by 30 nm and 310 nm along their short and long axes, respectively. As the length of the rods is decreased, the resonance frequency is blue shifted. From the point of view of the circuit theory approach, making the antennas shorter decreases their inductance and therefore increases the resonance frequency. According to the coupled plasmon theory, decreasing the length decreases the resonant wavelength due to the boundary condition. This length dependence is also consistent with the finding of Yu et. al. for aqueous solutions of suspended gold nano rods[22], and also with Ebbesen, for inductive FFSs[6], both of whom reported blue shifts in resonance corresponding to decreased aspect ratios (length/thickness).

An array with 2L = 140 nm, D_y = 100 nm, D_x = 120 nm, W = 60 nm, and a thickness of 50 nm (solid curve in 5a) was used to verify the off-normal affects on the reflectance spectrum predicted by the PMM model. Equation 4, 6, and 7 predict that the FWHM of the resonance should decrease by a factor of one half when $\theta = 60^o$ and that it should increase by a factor of two when $\phi = 60^o$ but the central wavelength should not change. Figures 6a and 6b show the simulated results for variations of θ and ϕ, respectively, with the other held constant. Figure 6c shows that the model does in fact agree with the PMM formulas to within about 24% for $\theta = 60^o$ and about 2% for $\phi = 60^o$. Compare these results with Figure 6d, which are the off-normal reflectance spectra from simulations of a tri-layer dielectric stack tuned to resonate at 460 nm. For a launch angle of 40° in either direction, the central wavelength blue shifts by 25 nm whereas for the FSS the central wavelength is constant up to 75° where it shifts by less than 10 nm. Additional simulations of five layer stack gave the same 25 nm shift at 40°. The magnitude changes that occur in Figure 6a and 6b are due to the variation in the Fresnel reflection coefficient at the air/ITO interface. For 6a the amplitude decreases as θ approaches Brewster's angle and for 6b it increases as ϕ becomes steeper[24]. These same trends were present in the dielectric stack data but were removed through normalization.

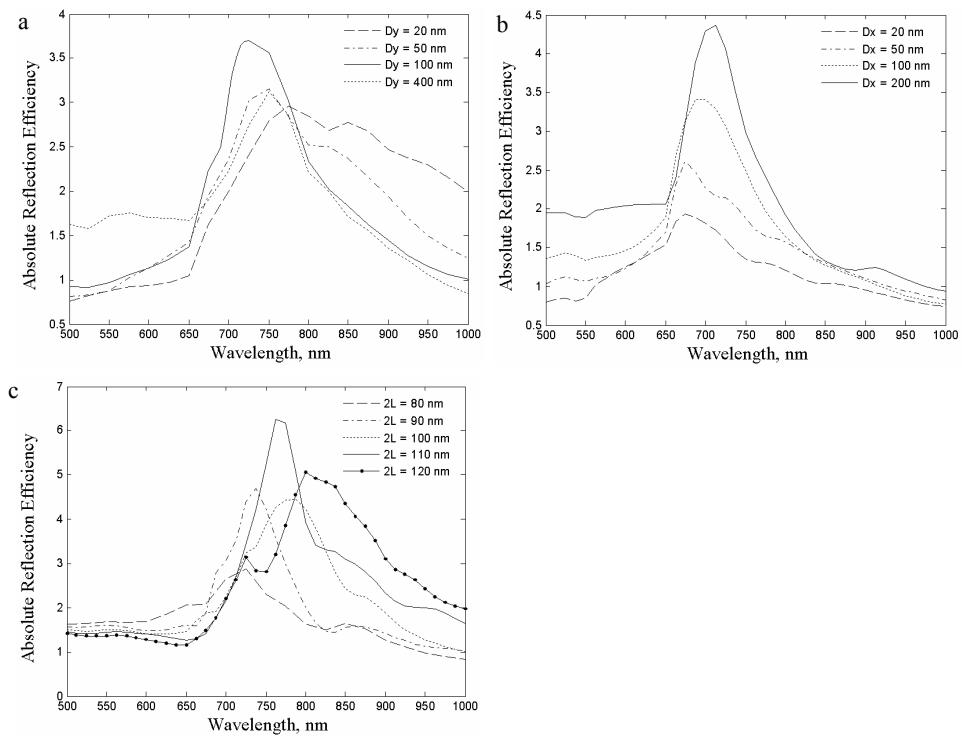

Figure 5: Simulated absolute reflection efficiency spectra of capacitive dipole FSSs of various dimensions. (a) The effects of changing the size of the gap along the long axis of the antennas. (b) The affect of changing the size of the gap along the short axis of the antennas. (c) The affects of changing the size of the length of the antennas. These results should be compared with those in Figure 4 of reference 4.

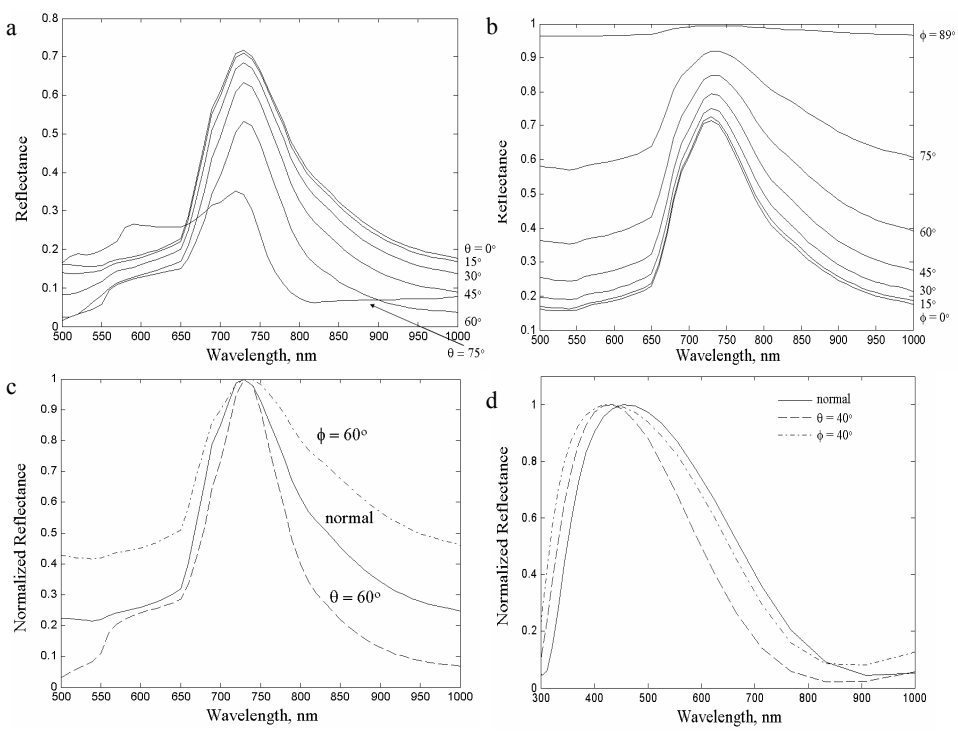

Figure 6: Simulations of off-normal affects on the reflectance spectrum. (a) Variation of θ in the E-k plane. (b) Variation of ϕ in the H-k plane. (c) Validation of MMP modal for θ = 60° and for ϕ = 60°. (d) Resonance shift for a tri-layer dielectric stack.

Finally, the affect of altering the polarization angle α was evaluated. Figure 7a shows the far-field reflectance at normal incidence as α is scanned from 0° (TM) to 90° (TE). The reflectance centered on the longitudinal resonance wavelength decreases as the angle increases. However, this decrease is relatively small over the first 15^0 and only decreases by 21% over the first 30°. The decrease occurs as expected as more of the electric field moves into the transverse direction. Simultaneously, a transverse plasmon mode is excited and a second resonance appears. The new peak is blue shifted from the original because the width of the antenna is shorter than the length. It also has much lower amplitude due to the long edge, which does not focus the charge density as the narrow rounded edge does. Figure 7b shows the reflectance spectrum for $\alpha = 0^o$, $\theta = 45^o$, and $\phi = 45^o$. In this case the electric field is half in the longitudinal direction and half in the transverse. The longitudinal resonance is identical in height and width to that of normal incidence with $\alpha = 45^o$ (7a), but the transverse resonance is much stronger indicating that the change in angle has increased the coupling efficiency to this plasmon mode.

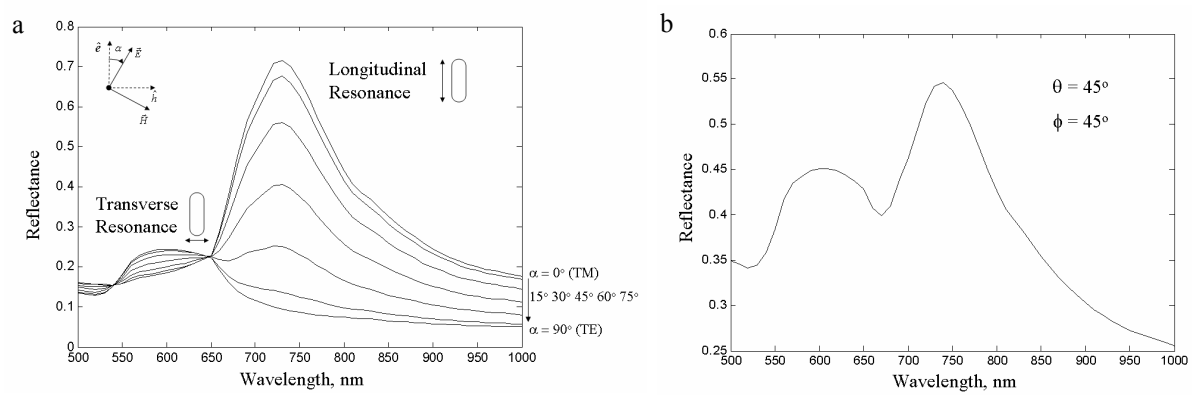

Figure 7: (a) Affect of polarization angle on the reflection spectrum. (b) Reflection spectrum when $\theta = 45^o$ and $\phi = 45^o$.

4. DEVICE FABRICATION AND FUTURE EXPERIMENTS

A FSS fashioned after the model described in the previous section was fabricated on a silicon substrate using electron beam (e-beam) lithography, physical vapor deposition, and lift-off in order to experimentally evaluate its off-normal properties. A 500 by 500 element nanoantenna array was defined using DesignCAD LT from Upperspace Corporation. Array dimensions were 2L = 140 nm, W = 60 nm, D_y = 100 nm, and D_x = 120 nm (refer to Figure 1). The pattern was defined in a 150 nm thick layer of PMMA (950k MW A2 Microchem) atop the silicon substrate using a Leica EBPG5HR e-beam tool at a bias of 100 kV and a beam current of 1 nA. In order to fill a large area it was necessary to stitch multiple patterns together. A laser-interferometer was used to align the stage to within +/- 30 nm between moves. Once the pattern was written, it was developed in a 1:1 solution of methyl-isobutyl ketone (MIBK) and Isopropanol (IPA) for 90 seconds, followed by 20 second rinse in IPA. It was then blown dry with nitrogen. After development, the sample was put through a descuming procedure in a Metroline low power oxygen plasma asher for 2 minutes to remove residue from the resist and substrate. The sample was then metallized in a CHA e-beam evaporator which deposited 10nm of chromium followed by 30nm of gold for a total thickness of 40nm. Finally, a lift-off procedure was used to remove the non-exposed PMMA, leaving behind the metallic antennas. The sample was immersed in a bath of 1-methyl-2-pyrrolidinone (NMP, Rohm-Hass Developer Microposit 1165) at 85˚C for 10 minutes, then rinsed in IPA and blown dry with nitrogen. The finished device was observed in a scanning electron microscope (SEM) to measure the nanoantenna feature sizes and completeness of the pattern/lift-off. An SEM image of the device is shown in Figure 8. Problems were encountered during the final lift-off that rendered the sample inadequate for subsequent experimental evaluation. Hence, it was not possible to complete the experimental portion of the study. A new sample is currently being fabricated, and once completed, will be used to experimentally validate the modeled results depicted in Figures 6 and 7. In addition to the macroscopic far-field reflectance properties, near-field enhancement and the underlying physical phenomenology which gives these devices their unique properties will be investigated.

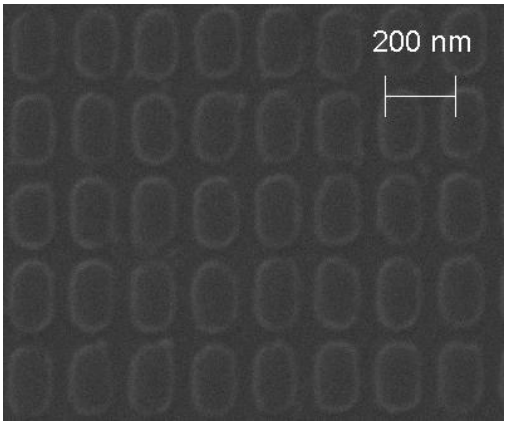

Figure 8: SEM image of gold nano-antenna array

5. DISCUSSION

The results of modeling reported in this study support the plausibility of scaling current RF and microwave FSS designs based on the analogous circuit model to the nano scale for use as NIR and visible filters. This model has been validated against experimental results for the far-field reflectance of capacitive FSSs at normal incidence and the off-normal excitation of surface plasmons in thin metal films. It has been used to study the scalability of off-normal trends predicted by the circuit model and the periodic moment method (PMM) for optical applications. The variation in the FWHM of the resonant peak in the reflection spectrum of a device illuminated by a TM polarized plane wave at an angle of 60° from normal in the E-k and H-k planes was found to agree with the PMM model to within 24.2% and 2.4% respectively. The largest potential advantage that FSS filters have over the currently available dielectric stacks is central wavelength stability over a wide range of launch angles. The simulations reported here show that for a launch angle of 75° from normal in the E-k and H-k planes the central wavelength shifts less then 10 nm in the blue and red directions respectively while that of three and five layer dielectric stack filters shifts by 25 nm at only 40°. The origin of this increased stability is that FSSs are comprised of horizontal cavities in which the propagation length does not change with launch angle as opposed to dielectric stacks, which are vertical cavities. Once fabrication of this device is complete these finding will be experimentally validated.

REFERENCES

[1] Munk, B., [Frequency Selective Surfaces Theory and Design], John Wiley & Sons, Inc., New York, Chapters 1 to 5 (2000)

[2] Ulrich, R., "Interference Filters for the Far Infrared", Applied Optics 7(9), 1987-1996 (1968)

[3] Crozier, K., Sundaramurthy, A., Kino, G., Quate, C., "Optical antennas: Resonators for local field enhancement", Journal of Applied Physics 94(7), 4632-4642 (2003)

[4] Smythe, E., Cubukcu, E., Capasso, F., "Optical properties of surface plasmon resonances of coupled metallic nanorods", Optics Express 15(12), 7439-7447 (2007)

[5] Cubukcu, E., Kort, E., Crozier, K., Capasso, F., "Plasmonic laser antenna", Applied Physics Letters 89, 09120 (2006)

[6] Ebbesen, T. W., Lezec, H. J., Ghaemi, H. F., Thio, T., Wolff, P. A., "Extraordinary optical transmission through sub-wavelength hole arrays", Nature 391, 667-669 (1998)

[7] Maier, S., Kik, P., Atwater, H., "Observation of coupled plasmon-polariton modes in Au nanoparticle chain waveguides of different lengths: Estimation of waveguide loss", Applied Physics Letters 81(9), 1714-1716 (2002)

[8] Hirsch, L., Stafford, R., Bankson, J., Sershen, S., Rivera, B., Price, R., Hazle, J., Halas, N., West, J., "Nanoshell-mediated near-infrared thermal therapy of tumors under magnetic resonance guidance", PANS 100(23), 13549-13554 (2003)

[9] Barnes, W., Dereux A., Ebbesen, T. W., "Surface plasmon subwavelength optics", Nature 424, 824-830 (2003)

[10] Prodan, E., Radloff, C., Halas, N., Nordlander, P., "A Hybridization Model for the Plasmon Response of Complex Nanostructures", Science 32, 419-422 (2003)
[11] Sambles, J., Bradbery, G., Yang, F., "Optical excitation of surface plasmons: an introduction", Contemporary Physics 32(3), 173-183 (1991)
[12] Chan, H. B., Marcet, Z., Carr, D., Bower, J. E., Cirelli, R., Ferry, E., Kelmens, F. P., Miner, J. F., Pai, C. S., Taylor, J. A., "Transmission Enhancement in an Array of Subwavelength Slits in Aluminum Due to Surface Plasmon Resonances", Bell Labs Tech. Journal 10, 143-150 (2005)
[13] Ritchie, R., Arakawa, E., Crowan, J., Hamm, R., "Surface-Plasmon Resonance Effect in Gration Diffraction", Physical Review Letters 21(22), 1530-1533 (1968)
[14] Palik, E., [Handbook of Optical Constants of Solids], Academic, New York, Volume 1, Page 294 (1985)
[15] RCWA software is DiffractMOD, Rsoft Design Group
[16] Li, L., "Use of Fourier series in the analysis of discontinuous periodic structures", Journal of the Optical Society of America A 13(9), 1870-1876 (1996)
[17] Haynes, C., McFarland, A., Zhao, L., Van Duyne, R., Schatz, G., Gunnarsson, L., Prikulis, J., Kasemo, B., Kall, M., "Nanoparticle Optics: The Importance of Radiative Dipole Coupling in Two-Dimensional Nanoparticle Arrays", Journal of Physical Chemistry B 107, 7337-7342 (2003)
[18] Kottmann, J., Martin, O., "Retardation-induced plasmon resonances in coupled nanoparticles", Optics Letters 26(14), 1096-1098 (2001)
[19] Rakic, A., Djurisic, A., Elazar, J., Majewski, M., "Optical properties of metallic films for vertical-cavity optoelectronic devices", Applied Optics 37(22), 5271-5283 (1998)
[20] Muhlschlegel, P., Eisler, H. J., Martin, O. J. F., Hecht, B., Pohl, D. W., "Resonant Optical Antennas", Science 308, 1607-1609 (2005)
[21] Sundaramurthy, A., Crozier, K., Kino, G., Fromm, D., Schuck, P., Moerner, W., "Field enhancement and gap-dependent resonance in a system of two opposing tip-to-tip Au nanotriangles", Applied Physics B 72, 165409 (2005)
[22] Yu, Y., Chang, S., Lee, C., Wang, C. R. C., "Gold Nanorods: Electrochemical Synthesis and Optical Properties", The Journal of Physical Chemistry B 101(34), 6661-6664 (1997)
[23] Fang, N., Lee, H., Sun, C., Zhang, X., "Sub–Diffraction-Limited Optical Imaging with a Silver Superlens", Science 308, 534-537 (2005)
[24] Hecht, E., [Optics], 3rd edition, Addison-Wesley, Chapters 3 and 4 (1998)